Biochemical and Biophysical Research Communications 432 (2013) 389–393

Contents lists available at SciVerse ScienceDirect

Biochemical and Biophysical Research Communications

journal homepage: www.elsevier.com/locate/ybbrc

Ex-vivo assessment and non-invasive in vivo imaging of internal hemorrhages in *Aga2/+* mutant mice

Vladimir Ermolayev [a], Christian M. Cohrs [b], Pouyan Mohajerani [a], Angelique Ale [a], Martin Hrabé de Angelis [b], Vasilis Ntziachristos [a,*]

[a] Institute for Biological and Medical Imaging, Helmholtz Zentrum München, Building 56, Ingolstädter Landstraße 1, D-85764 Neuherberg, Germany
[b] Institute for Experimental Genetics, Helmholtz Zentrum München, Ingolstädter Landstraße 1, D-85764 Neuherberg, Germany

ARTICLE INFO

Article history:
Received 3 January 2013
Available online 18 January 2013

Keywords:
Osteogenesis imperfecta
Hemorrhages
Fluorescence molecular tomography
X-ray computer tomography
Vascular contrast agent
Collagen mutation

ABSTRACT

Mutations in type I collagen genes (COL1A1/2) typically lead to *Osteogenesis imperfecta*, the most common heritable cause of skeletal fractures and bone deformation in humans. Heterozygous *Col1a1*$^{Aga2/+}$, animals with a dominant mutation in the terminal C-propeptide domain of type I collagen develop typical skeletal hallmarks and internal hemorrhages starting from 6 day after birth. The disease progression for *Aga2/+* mice, however, is not uniform differing between severe phenotype lethal at the 6–11th day of life, and moderate-to-severe one with survival to adulthood. Herein we investigated whether a new modality that combines X-ray computer tomography with fluorescence tomography in one hybrid system can be employed to study internal bleedings in relation to bone fractures and obtain insights into disease progression. The disease phenotype was characterized on *Aga2/+* vs. wild type mice between 6 and 9 days postnatal. Anatomical and functional findings obtained in-vivo were contrasted to the ex-vivo appearance of the same tissues under cryo-slicing.

1. Introduction

Osteogenesis imperfecta (OI) is the most common heritable cause of skeletal fractures and bone deformations in humans. The more prevalent autosomal dominant forms of OI are caused by primary defects in type I collagen genes (*COL1A1*/*COL1A2*), whereas autosomal recessive forms are caused by deficiency of proteins which interact with type I procollagen for post-translational modification and/or folding [1,2]. The *Aga2* (abnormal gait 2) mouse model for human OI bearing a mutation in the corresponding terminal C-propeptide region of COL1A1 was recently discovered [3]. *Col1a1*$^{Aga2/+}$ animals demonstrated altered skeletal phenotype already at birth and possessed markedly increased bone turnover as well as disrupted native collagen network. The disease progression for *Col1a1*$^{Aga2/+}$ mice with the same genotype were not uniform. Some of the animals were severely affected (*Aga2*^{severe}) developing a lethal phenotype until the 6–11th day of life, which was characterized by thin calvaria, hemorrhages in different regions including thorax, joint cavities and brain, scoliosis, provisional rib and long bone calluses and deformities, body size deficits [3]. Other animals displayed dystrophic limb(s), long bone and pelvis fractures and moderately reduced body size, but survived to adulthood and were classified as moderately-to-severely affected (*Aga2*^{mild}). One of the hallmarks detectable on the histological sections was the appearance of internal hemorrhages in the thorax area [4], which reflected the excessive bleedings and easy formation of hemorrhages, reported for different patients suffering from OI [5].

Post-mortem methods of analysis including assessment of histological sections and immunohistochemistry typically confirms the presence of internal bleeding but cannot capture the time-course of disease development. Moreover, ex-vivo analysis is generally invasive and it therefore may induce discrepancies on the in-vivo conditions. Among various in vivo imaging techniques that could reveal lung bleeding in-vivo, Magnetic Resonance Imaging (MRI) or Ultrasound Imaging (US) are not ideally suited for imaging the lung. Nuclear imaging methods typically utilize short-lived radio-chemicals that make longitudinal imaging challenging. Instead we selected to investigate herein a novel hybrid fluorescence molecular tomography (FMT) and X-ray computer tomography (XCT) system [6]. FMT–XCT is an imaging method developed for three-dimensional in-vivo visualization of anatomical and functional tissue parameters [7], and offers a range of new capabilities for studying biological functions. One of the key advantages for this imaging modality is the seamless co-registration of XCT anatomical and FMT functional contrast information [8,9], which could be utilized to study lung bleedings.

Correspondingly, we administered a vascular fluorescence contrast agent to evaluate internal hemorrhages in the thorax area of *Col1a1*$^{Aga2/+}$ and wild type (WT) mice in order to better understand

* Corresponding author. Fax: +49 (0) 89 3187 3008.
E-mail address: v.ntziachristos@tum.de (V. Ntziachristos).

0006-291X/$ - see front matter © 2013 Elsevier Inc. All rights reserved.
http://dx.doi.org/10.1016/j.bbrc.2013.01.011

the disease development between 6th and 9th days postnatal. We explored whether FMT–XCT can be employed to characterize lung bleedings in-vivo, through the intact animal and differentiate between severe and moderate disease phenotypes. To confirm the in-vivo findings we subjected animals to a three-dimensional fluorescence cryo-slicing imaging protocol recently developed [10], which imaged the animals ex vivo in high resolution.

2. Materials and methods

2.1. Animals, contrast agents and validation experiments

Col1a1$^{Aga2/+}$ mice aged between 6 and 9 days postnatal [3] were used in this work. 2 nmoles of AngioSense (Perkin Elmer Waltham, MA, USA) contrast agent was injected intraperitoneally (i.p.) 1.5 h prior to the imaging through fluorescence molecular tomography coupled with X-ray computer tomography (FMT–XCT). AngioSense is a near-infrared in vivo blood pool fluorescent imaging agent, which can remain in the vasculature for several hours. During the imaging, the animals were anesthetized by isoflurane inhalation. All procedures with animals were performed in agreement with Helmholtz Zentrum Munich and Government of Bavaria as well as international laws and regulations. After in-vivo imaging, the animals were euthanized and frozen to −80 °C for further validation and analysis.

Frozen animals were sliced through the thorax area and imaged every 250 μm using a Multispectral Epi-Illumination Cryoslicing Imaging system as described elsewhere [10]. The multispectral epi-fluorescence imaging system included a 250 W white light source (KL2500 LCD, Carl Zeiss AG, Oberkochen, Germany) coupled via a flexible fiber bundle to a filter wheel (FW102B, Thorlabs, Newton, NJ, USA), which controlled the selection of excitation filters. A sensitive, high-resolution CCD camera (PCO AG, Donaupark, Kelheim, Germany), a zoom objective (Nikkor 24–85 mm, Tokyo, Japan), and a custom 10-position filter wheel (Cairn Research Ltd., Kent, UK) capture reflectance and fluorescence images at multiple spectral bands with a field of view that can range from 64 × 46 to 18 × 13 mm. The imaging system was mounted onto a rotary cryotome (CM 1950, Leica Microsystems GmbH, Wetzlar, Germany). Specially designed software and algorithms developed using Matlab (Mathworks, Natick, MA, USA) and LabView (National Instruments, Austin, TX, USA) control the sectioning procedure of the cryotome and trigger the image acquisition of the optical system [10]. The fluorescence images were normalized with respect to the exposure time for all the animals studied. Fluorescence images obtained from each slide are presented as color overlays over grayscale photographs of the same slice.

2.2. FMT–XCT hybrid system

The imaging of the mice was done using a prototype FMT–XCT hybrid imaging system developed by our group [8,9,11]. Briefly, the hybrid imaging system integrated a fluorescence molecular tomography FMT [7] into a commercial micro X-ray computed tomography system (eXplore Locus, General Electric HealthCare, London, ON, Canada). The FMT and XCT components were mounted on a common rotating gantry of 1 m diameter. FMT imaging could be performed in two wavelengths, by employing two laser diodes sources at 670 nm and 750 nm (B&W Tek, Newark, DE) with maximum optical power of 300 mW. Fluorescence images at different wavelengths were obtained by switching appropriate band-pass filters in-front of a CCD camera (Pixis 512; Roper Scientific Princeton NJ) which was placed on the opposite site of the optical source to image mice in transillumination mode, over 360° angles. The mice were anesthetized by isoflurane inhalation during all in-vivo FMT–XCT imaging experiments. Image reconstruction was based on an inversion technique that utilizes XCT priors in modeling photon propagation in tissues and during the inversion process in order to improve the accuracy of the FMT problem, as reported in Ref. [6].

3. Results

AngioSense is a fluorescent in-vivo blood pool imaging agent, which enables visualization of blood vessels and angiogenesis. In case of bleeding event AngioSense leaves the vasculature and labels the blood depots, which are being developed at the time of experiment, i.e. active bleeding sites. Initially, we experimentally defined the AngioSense application scheme suitable for the analysis of internal hemorrhages in *Aga2/+* mice (for the details, see Section 2).

Fig. 1 shows ex-vivo analysis of AngioSense fluorescence distribution in 6-day-old mouse pups (red color superimposed on the black and white cross sections; the color intensity corresponds to the fluorescence signal intensity, see the scale). Sites of rib breakages and remodeling as a primary hallmark of OI were never found in WT, but were clearly visible in *Aga2/+* mice (Fig. 1, asterisks). Detectable levels of AngioSense fluorescence were also not found in the thorax area of WT animals. Intensive active bleeding sites on the contrary were shown in *Col1a1*$^{Aga2/+}$ mice by AngioSense fluorescence signal, as was depicted on Fig. 1, AngioSense. The *Col1a1*$^{Aga2/+}$ mice with identical genotype demonstrated variability in spatial signal distribution. Mildly affected *Aga2*^{mild} showed the tendency to the localization of the bleeding sites in the edges of lungs and in the vicinity of bone remodeling (Fig. 1, *Aga2*^{mild}, arrows) along with lower bleeding intensity in the rest of the thorax. *Aga2*^{severe} mice, which showed signs of severe phenotype, e.g. reduced weight and ataxic behavior demonstrated higher AngioSense intensity and more diffuse bleeding pattern showing massive internal bleedings in the whole thorax area (Fig. 1, *Aga2*^{severe}). The major bleedings could be seen as blood depots (Fig. 1, arrows), but analysis of color images (Fig. 1, Color) did not show the active hemorrhage distribution, which confirms the discrepancies between blood depots and the bleeding sites specifically visualized upon application of the contrast agent.

Fig. 2 summarizes the AngioSense fluorescence distribution analysis ex vivo in 9-day-old pups. Similar to 6-day-old ones, neither bone remodeling areas nor AngioSense fluorescence were detected in the WT. Profound difference in the distribution of active bleedings visualized by the contrast agent was observed for *Col1a1*$^{Aga2/+}$ mice. Fig. 2 shows that contrast agent level in thorax of mildly affected *Aga2*^{mild} mice was lower than for the 6-day-old mice (AngioSense panel). Major bleedings (Fig. 2, the arrows and the color for the signal intensity) were concentrated in the vicinity to the bone remodeling sites (Fig. 2, asterisks) and on the edge of the lungs. Different pattern was seen for the *Aga2*^{severe} mice. Intensive fluorescence was found in the periphery of thorax area (Fig. 2, AngioSense, *Aga2*^{severe}, arrows), but not in the middle of thorax area as it was observed for the 6-day-old animals.

The difference in bleeding pattern could be best recognized on the 3D reconstruction of the cryo-slicing image stacks. The fluorescence signal was concentrated in the vicinity of bone remodeling for *Aga2*^{mild} mice and very intense fluorescence was present through the periphery of the whole thorax area for *Aga2*^{severe} animals (Fig. 2, AngioSense: 3D reconstruction). The lower panel of the Fig. 2 shows the corresponding color images. The analysis of the color images along with visual control during the slicing experiment showed a lot of blood in the lungs of severely affected mice (Fig. 2, *Aga2*^{severe}), which also corresponded with histological analysis. As for 6-day-old pups, color images did not reveal active bleeding sites visualized upon AngioSense application.

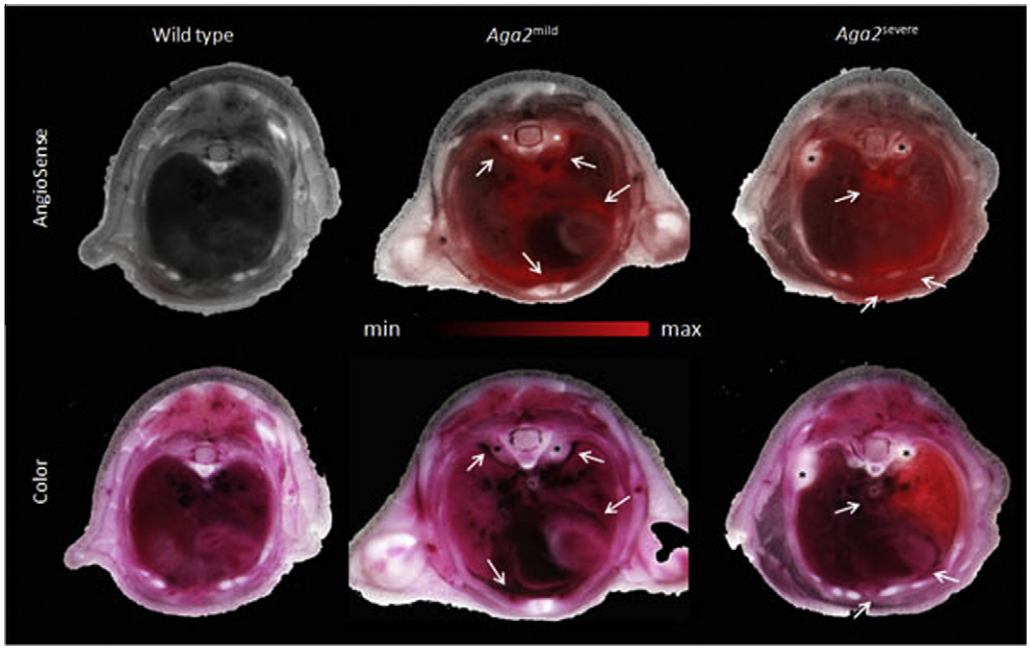

Fig. 1. Reconstruction of AngioSense spatial distribution in 6-day-old wild type and *Aga2/+* mice indicating areas of internal bleedings (red, arrows). Upper panel: reconstructions of AngioSense spatial distribution. Wild type animals demonstrated very low/no AngioSense fluorescence. *Aga2/+* mice demonstrated discrepancy in bleeding intensity and distribution. Mildly affected *Aga2/+* mice showed localized pattern of internal bleedings. Some of them were located near bone breakage areas (seen by thicker bone remodeling sites, asterisks). Other bleeding areas were not in the vicinity of broken bones. Severely affected mice showed intensive hemorrhages in the whole thorax area. The reconstructions were done using AngioSense fluorescence and color images of serial transversal cryo-sections and normalized to the wild type. Lower panel: corresponding color images, which represent not the active bleeding sites, but rather can be used to compare lung anatomy and general blood content. (For interpretation of the references to color in this figure legend, the reader is referred to the web version of this article.)

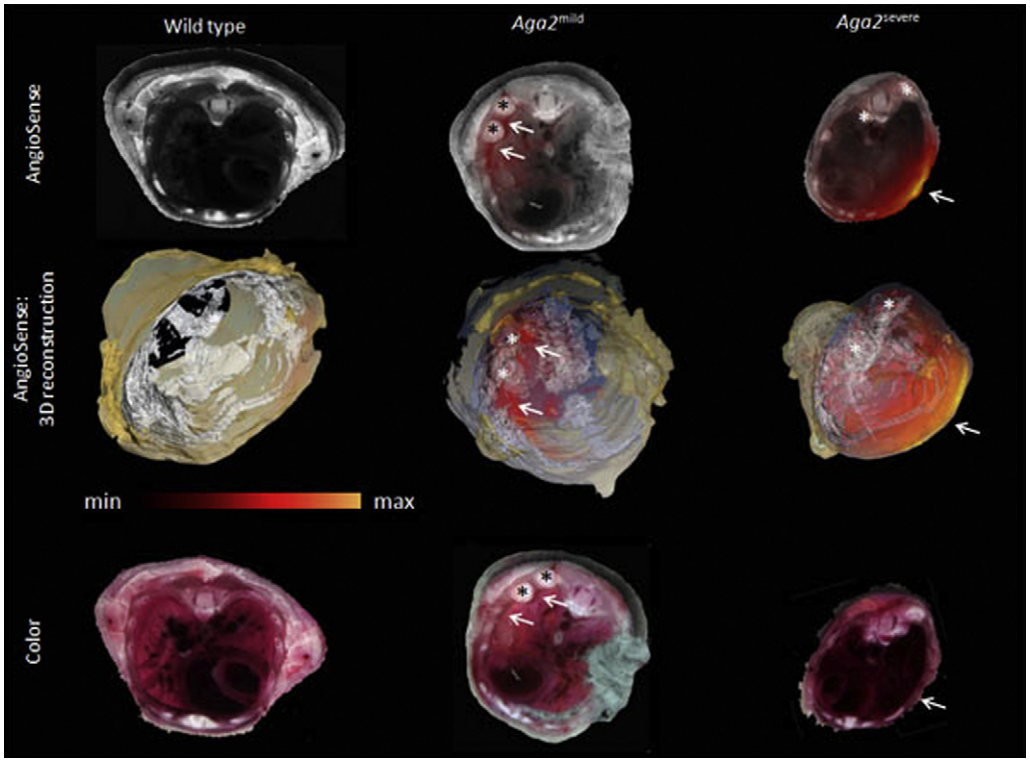

Fig. 2. Reconstruction of AngioSense spatial distribution in 9-day-old wild type and *Aga2/+* mice showing the areas of internal bleedings (red color showing the intensity of fluorescence signal, arrows indicate the bleeding sites). Upper panel: 2D co-registration of anatomical black and white image and AngioSense fluorescence. Small boxes: corresponding color images showing dark red lungs for *Aga2/+* severe mice indicating high blood content. Lower panel: 3D reconstruction of thorax area based on the serial transversal cryo-sections. Wild type animals demonstrated very low/no AngioSense fluorescence. Mildly affected *Aga2/+* mice showed pattern of internal bleedings similar to 6-day-old ones. The severely affected mice showed bleedings only on the periphery of thorax area. The reconstructions were done by overlaying AngioSense and anatomical black and white images of serial transversal cryo-sections. Color scale shows indicates the intensity of AngioSense fluorescence signal. (For interpretation of the references to color in this figure legend, the reader is referred to the web version of this article.)

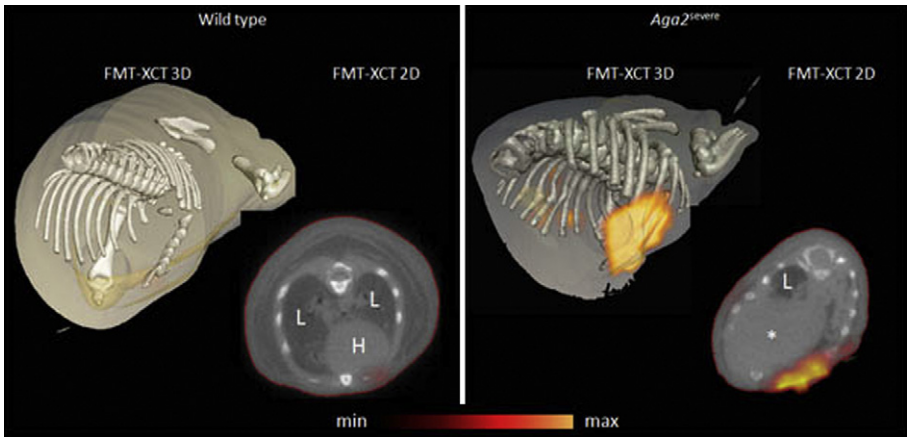

Fig. 3. In vivo evaluation of active bleeding sites in 9-day-old animals using FMT-XCT imaging. FMT-XCT reconstructions revealed no AngioSense fluorescence in thorax area of WT animals (L – lung; H – heart). Blood occupying almost the whole thorax area (asterisk) was detected in *Aga2/+* severely affected mice. High AngioSense fluorescence (red to yellow color showing quantitative evaluation of fluorescence signal) indicating active bleeding sites could be detected in the periphery of thorax area of *Aga2/+* severely affected mice. (For interpretation of the references to color in this figure legend, the reader is referred to the web version of this article.)

In order to better understand spatial distribution of hemorrhages and explore, whether they can be detected in-vivo, we performed non-invasive hybrid FMT–XCT imaging for 9-day-old pups. Fig. 3 demonstrates the reconstruction of image stacks for AngioSense fluorescence by FMT channel co-registered with anatomical information obtained by XCT imaging. Reconstruction of the XCT channel data demonstrated massive blood deposition in the lungs of $Aga2^{severe}$ mice, but not in the WT (Fig. 3, $Aga2^{severe}$, asterisk), which corresponded to the ex vivo data (Fig. 2, $Aga2^{severe}$). FMT data on AngioSense distribution revealed that the intensive active bleedings were localized in the periphery of thorax area Aga2/+ animals (Fig. 3, $Aga2^{severe}$), which also corresponded well with the validation images obtained by cryo-slicing. WT mice did not show AngioSense localization neither in-vivo nor in ex-vivo validation experiments. It has to be noted that mildly affected $Aga2^{mild}$ animals showed quite weak signal in the FMT–XCT imaging experiments, which correlated well with the cryo-slicing data and was masked in-vivo by the strong fluorescence from the liver.

4. Discussion

Along with bone fragility and defects, excessive bruising and general bleeding problems belong to a well recognized feature of human OI, which was well documented by several medical case reports [5,12,13]. The pioneering work on the $Col1a1^{Aga2/+}$ mouse model of OI revealed the critical features of its phenotypes, such as increased bone fractures, osteoporosis, disorganized trabecular and collagen structures. These features occurred already at birth closely correlating to OI type II-III [3]. It was also noted that $Col1a1^{Aga2/+}$ mice with the same genotype develop different phenotypes, one of them $Aga2^{mild}$ representing mildly affected animals with moderate features of OI, which could survive to adulthood. $Aga2^{severe}$ mice developed the second phenotype displaying severe progression of OI, which led to premature death between 6 and 11 days postnatal. The recent report documented cardiopulmonary dysfunction in Aga2/+ mice, inter alia the bleedings in the thorax as well as primary structural and intrinsic cellular defects in hearts of $Aga2^{severe}$ mutant mice [4].

In this work, we concentrated on the investigation of internal hemorrhages in $Col1a1^{Aga2/+}$ mice developing different phenotypes between 6th and 9th day of life. Ex vivo macroscopic and microscopic histological analyses could reveal merely the cumulative blood content, which occured up to the time point of animal sacrifice, but were not able neither assess the active processes nor distinguish between active and non-active bleedings. Therefore we applied the fluorescent intravital blood pool contrast agent AngioSense to quantitatively visualize active internal bleedings in-vivo and ex vivo. Active bleedings and already formed blood depots could be macroscopically localized in the thorax area in both $Aga2^{mild}$ and $Aga2^{severe}$ mice at 6 days of age (Fig. 1, arrows). The comparison between spatial localization of active bleeding sites visualized by AngioSense and color images confirmed that active hemorrhages were only partially detectable by plain imaging. The hemorrhages of varying intensity were spread in the entire thorax area (Fig. 1, the red color for AngioSense signal distribution). $Aga2^{mild}$ mice showed the tendency for the major bleeding localization in the lung periphery and in the vicinity of bone breakage and remodeling (Fig. 1, asterisks) along with less intensive hemorrhages in the rest of the lungs. $Aga2^{severe}$ animals demonstrated intensive diffuse bleeding pattern within the whole thorax (Fig. 1, $Aga2^{severe}$).

$Col1a1^{Aga2/+}$ mice at 9 days of age showed more profound difference in active bleeding distribution pattern. Major bleeding sites for $Aga2^{mild}$ phenotype did occur in the lung periphery and in the vicinity of the bone remodeling. The intensity of bleeding was lower than for the 6-day-old mice and less intense in the rest of the lung. Some hemorrhages could be attributed to the tissue damage upon bone breakages, however bleedings also occurred not in the vicinity of the bone breakage sites. $Aga2^{severe}$ mice showed very high blood content in the lungs at 9 days of age, which could be detected on the color cryo-slicing images (Fig. 2, Color) and was also confirmed by in-vivo XCT channel (Fig. 3, asterisk). In-vivo XCT data also ruled out possible slicing and sample preparation artifacts. Intensive active bleedings were found only on the periphery of the thorax area. Blood possibly accumulated between 6 and 9 days postnatal and occupied the majority of the lung space. The bleedings still persisted at 9 days of age, however only in the periphery. This conclusion is also supported by the comparison between fluorescence and color imaging, the first showing the active bleeding sites and latter – resulting blood content. The analysis of FMT–XCT in-vivo imaging also revealed intensive internal hemorrhages located in the periphery of thorax area (Fig. 3, color scale) and massive blood content in the lungs of $Aga2^{severe}$ mice (Fig. 3, asterisk),

Our results suggest that internal hemorrhages developed primarily due to the vasculature properties of $Col1a1^{Aga2/+}$ animals, but also could accompany the bone breakage events. This observation is in agreement with recent study reporting the bleedings in $Aga2^{severe}$ mice based on macroscopic observation and histological

analysis [4]. Our study showed the active bleedings in *Aga2*^{severe} and *Aga2*^{mild} pups and demonstrated the developing discrepancies between mild and severe phenotypes, which were already visible at 6 days of age and were quite profound at 9 days. The development of intensive bleedings and accumulation of large amounts of blood in the thorax area may contribute to death of *Aga2*^{severe} mice at 6–11th day postnatal.

The majority of the studies into OI were concentrated on alterations in bone structure and properties, however recent studies start addressing also cardiovascular and pulmonary dysfunctions in animal models and patients of OI [4]. Due to the numerous reports over the bleedings during the surgeries and the ready bleeding problems as well as hematoma formation in response to minor traumas in the patients suffering from OI [5,12–16], the analysis of hemorrhages is very important in understanding OI development and symptoms, and developing effective therapies. This study demonstrated that the intensity and spatial distribution of the bleedings may play a significant role in the development of different phenotypes of *Col1a1*$^{Aga2/+}$ mice and contribute to survival of *Aga2*^{mild} and to premature death of *Aga2*^{severe}. We also showed for the first time that the active internal bleedings in OI model could be successfully imaged and assessed in-vivo (Fig. 3). These experiments showed that FMT–XCT imaging modality and reconstruction combined with application of in vivo fluorescent contrast agent has a potential for non-invasive research and diagnostic applications such as correct detection of bone remodeling and internal hemorrhage sites.

Acknowledgments

The authors would like to thank Claudia Mayerhofer, Sarah Glasl and Florian Jurgeleit for the technical assistance. This work was supported by German Federal Ministry of Education and Science (BMBF) research grant MOBIMED (Molecular Imaging in Medicine).

References

[1] A. Forlino, W.A. Cabral, A.M. Barnes, J.C. Marini, New perspectives on osteogenesis imperfecta, Nat. Rev. Endocrinol. 7 (9) (2011) 540–557.
[2] J.C. Marini, A. Forlino, W.A. Cabral, A.M. Barnes, J.D. San Antonio, S. Milgrom, J.C. Hyland, J. Korkko, D.J. Prockop, A. De Paepe, P. Coucke, S. Symoens, F.H. Glorieux, P.J. Roughley, A.M. Lund, K. Kuurila-Svahn, H. Hartikka, D.H. Cohn, D. Krakow, M. Mottes, U. Schwarze, D. Chen, K. Yang, C. Kuslich, J. Troendle, R. Dalgleish, P.H. Byers, Consortium for osteogenesis imperfecta mutations in the helical domain of type I collagen: regions rich in lethal mutations align with collagen binding sites for integrins and proteoglycans, Hum. Mutat. 28 (3) (2007) 209–221.
[3] T.S. Lisse, F. Thiele, H. Fuchs, W. Hans, G.K. Przemeck, K. Abe, B. Rathkolb, L. Quintanilla-Martinez, G. Hoelzlwimmer, M. Helfrich, E. Wolf, S.H. Ralston, M.H. de Angelis, ER stress-mediated apoptosis in a new mouse model of osteogenesis imperfecta, PLoS Genet. 4 (2) (2008) e7.
[4] F. Thiele, C.M. Cohrs, A. Flor, T.S. Lisse, G.K. Przemeck, M. Horsch, A. Schrewe, V. Gailus-Durner, B. Ivandic, H.A. Katus, W. Wurst, C. Reisenberg, H. Chaney, H. Fuchs, W. Hans, J. Beckers, J.C. Marini, M. Hrabe de Angelis, Cardiopulmonary dysfunction in the Osteogenesis imperfecta mouse model Aga2 and human patients are caused by bone-independent mechanisms, Hum. Mol. Genet. (2012).
[5] G. Edge, B. Okafor, M.E. Fennelly, A.O. Ransford, An unusual manifestation of bleeding diathesis in a patient with osteogenesis imperfecta, Eur. J. Anaesthesiol. 14 (2) (1997) 215–219.
[6] A. Ale, V. Ermolayev, E. Herzog, C. Cohrs, M. Hrabe de Angelis, V. Ntziachristos, FMT–XCT: in vivo animal studies with hybrid fluorescence molecular tomography–X-ray computed tomography, Nat. Methods 9 (6) (2012) 615–620.
[7] V. Ntziachristos, C.H. Tung, C. Bremer, R. Weissleder, Fluorescence molecular tomography resolves protease activity in vivo, Nat. Med. 8 (7) (2002) 757–760.
[8] A. Ale, R.B. Schulz, A. Sarantopoulos, V. Ntziachristos, Imaging performance of a hybrid x-ray computed tomography–fluorescence molecular tomography system using priors, Med. Phys. 37 (5) (2010) 1976–1986.
[9] R.B. Schulz, A. Ale, A. Sarantopoulos, M. Freyer, E. Soehngen, M. Zientkowska, V. Ntziachristos, Hybrid system for simultaneous fluorescence and x-ray computed tomography, IEEE Trans. Med. Imaging 29 (2) (2010) 465–473.
[10] A. Sarantopoulos, G. Themelis, V. Ntziachristos, Imaging the bio-distribution of fluorescent probes using multispectral epi-illumination cryoslicing imaging, Mol. Imaging Biol. (2010).
[11] M. Freyer, A. Ale, R.B. Schulz, M. Zientkowska, V. Ntziachristos, K.H. Englmeier, Fast automatic segmentation of anatomical structures in x-ray computed tomography images to improve fluorescence molecular tomography reconstruction, J. Biomed. Opt. 15 (3) (2010) 036006.
[12] Y. Endo, S. Mamiya, H. Niitsu, Hemorrhagic diathesis in van der Hoeve's syndrome, Arch. Intern. Med. 144 (9) (1984) 1889–1893.
[13] B.M. Siegel, I.A. Friedman, S.O. Schwartz, Hemorrhagic disease in osteogenesis imperfecta; study of platelet functional defect, Am. J. Med. 22 (2) (1957) 315–321.
[14] H.M. Haddad, Hemorrhages after minor trauma, Ophthalmology 112 (4) (2005) 737–738.
[15] C.D. Parmar, A.K. Sinha, C. Hayhurst, P.L. May, D.F. O'Brien, Epidural hematoma formation following trivial head trauma in a child with osteogenesis imperfecta. Case report, J. Neurosurg. 106 (Suppl. 1) (2007) 57–60.
[16] D. Sasaki-Adams, A. Kulkarni, J. Rutka, P. Dirks, M. Taylor, J.M. Drake, Neurosurgical implications of osteogenesis imperfecta in children. Report of 4 cases, J. Neurosurg. Pediatr. 1 (3) (2008) 229–236.